



**Faculty of sciences
Physics section
End of degree thesis**

**Determination of the physical parameters of eclipsing binary star systems
ASASSN-VJ050229.84-052203.4 and CRTSJ041918.8-071807**

Written by:
Gareb Enoc Fernández Rodríguez

Supervised by:
María Jesús Arévalo Morales
Enric Pallé Bago

July 2023

Resumen

En este trabajo se presentan los resultados del análisis de las curvas de luz de dos estrellas binarias ASASSN-VJ050229.84-052203.4 y CRTSJ041918.8-071807. Las observaciones de ASASSN-VJ050229.84-052203.4 se hicieron con el telescopio IAC80 y las de CRTSJ041918.8-071807 con el telescopio Carlos Sánchez, ambos del Observatorio del Teide.

En la introducción se da una visión general de las estrellas binarias, en especial las binarias eclipsantes desarrollando las expresiones que permiten obtener valores de los parámetros físicos de las dos componentes del sistema.

En el capítulo 2 se hace una descripción de la instrumentación que incluye los telescopios así como las CCD utilizadas. Se describen los pasos para la reducción de los datos con los programas utilizados. También en este capítulo se describen los programas de desarrollo propio que se han elaborado para el análisis de las curvas de luz. El capítulo termina con una clasificación espectral preliminar de las componentes de los sistemas. Esta clasificación indica que ASASSN-VJ050229.84-052203.4 es una binaria con curva de luz tipo Algol y componentes A9V y K2V. Los colores publicados de CRTSJ041918.8-071807 indican que las dos estrellas son de tipo M3V y M4.5V. A pesar de su periodo orbital de menos de 6 horas parece un sistema separado con dos estrellas poco masivas, de menos de 1 masa solar.

En el capítulo 3 se presentan los resultados preliminares del análisis de las curvas utilizando la versión más actual el código Phobe.

Los capítulos finales 4 y 5 se dedican a la discusión de los parámetros orbitales obtenidos y a las conclusiones que se han sacado en este trabajo. Se finaliza con una propuesta de observaciones , fotométricas y espectroscópicas que serían necesarias obtener en un futuro para poder determinar con absoluta fiabilidad los valores de los parámetros físicos y comparar con modelos de evolución.

Contents

1	Introduction	4
1.1	Binary star systems	4
1.2	Eclipsing binaries	4
1.3	Main parameters of eclipsing binary star systems	5
1.3.1	Light curves	6
1.3.2	Radial velocity curves	9
1.4	Different types of eclipsing binaries	11
1.4.1	Algol type	11
1.4.2	Beta Lyrae	11
1.4.3	W Ursae Majoris	12
2	Observations and data reduction	13
2.1	Observations	13
2.1.1	ASASSN-VJ050229.84-052203.4	13
2.1.2	CRTSJ041918.8-071807	14
2.2	Telescopes and instruments	16
2.2.1	IAC80 - CAMELOT2	16
2.2.2	TCS - MuSCAT2	17
2.3	Data correction	17
2.3.1	Bias	17
2.3.2	Flat-Fields	17
2.3.3	Darks	18
2.3.4	Image correction	18
2.4	Photometry	18
2.4.1	Astrometry	19
2.4.2	Aperture photometry with PyRAF and PhotUtils	20
3	Lightcurve modelling	26
3.1	PHOEBE2	26
3.2	Lightcurve modelling of ASAS05 and CRTS04 stars	27
3.2.1	ASAS05	27
3.2.2	CRTS04	28
3.2.3	Nelder-Mead optimization	28
4	Results	31
4.1	Orbital and stellar parameters	31
4.2	Classification and H-R diagram	33

5	Final conclusions	35
5.1	Summary of the results obtained	35
5.2	Future work	36

Chapter 1

Introduction

En este capítulo introductorio se explicará brevemente lo que son los sistemas binarios eclipsantes, tipos y el interés científico para su estudio. Se darán unas nociones acerca de cuales son los principales parámetros que los describen.

1.1 Binary star systems

Most stars that can be seen by eye appear to be just a point in the sky. However this is not always the case. Sometimes stars form in binary, triple or even quadruple star systems. The first binary star systems observed with telescopes date back to the middle of the seventeenth century, observed by astronomers such as Giovanni Battista Riccioli. For these early observations most of the discovered “double stars” were visual binaries, which are stars that appear nearby in the sky but in which the semi major axis of the orbit is large due to the long orbital period. During the late eighteenth and early nineteenth century astronomers such as John Michell and William Herschel proposed and tested respectively the existence of double stars. The nature of these systems can be varied as there are many classifications depending on certain characteristics like the orbital inclination or the type of stars present.

1.2 Eclipsing binaries

Some stars were seen for many years to decrease in brightness with a given periodicity but the cause was unknown. It was not until 1889 that the first eclipsing binary was discovered in the Algol system by John Goodricke. These eclipsing binaries are formed by two or more stars orbiting the center of mass, or barycenter, of the system crossing in front of one another from our line of sight. More specifically, the inclination of the orbit is close to 90° in the case of detached binaries so it aligns with our line of vision and we can see them edge on. These stars are usually not seen individually because they are too close to each other to be resolved by telescopes but we can extract great amounts of information from these systems, in fact binaries, and more specifically eclipsing and spectroscopic binaries are the only way to accurately estimate stellar parameters. One example of these parameter may be that of the mass. From Newton’s second law it follows that there is a relationship between mass and acceleration. So in order to correctly measure the mass of one star you need another object massive enough to create changes in its acceleration, in most cases this will be another companion star. Nowadays we know that it is not uncommon for stars to be in double or triple systems and in fact the number of eclipsing binaries in catalogues such as ASAS-SN catalogue are in the tens of thousands, Christy et al. (2023).

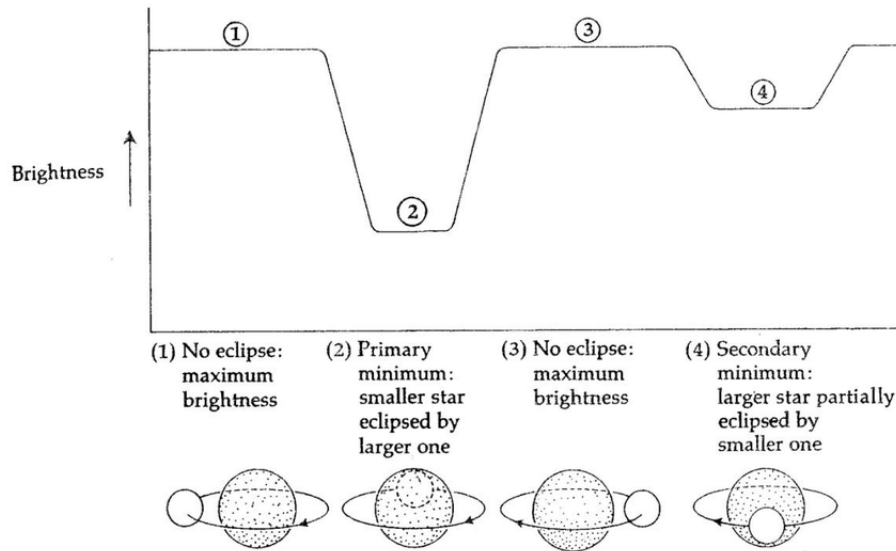


Figure 1.1: Example of the light curve of an eclipsing binary star system, taken from Hani et al. (2014).

1.3 Main parameters of eclipsing binary star systems

To fully characterise a binary star's orbit we need to provide the following 7 orbital elements: a , the semi major axis, e , the eccentricity of the orbit, i , the orbital inclination, Ω , the longitude of the ascending node, ω , the argument of periastron, T_0 , the time of a primary minimum and P , the orbital period, Taff (1985), Moulton (1984). However some of these elements such as the semi major axis cannot be calculated with precision without radial velocity curves. Most of these parameters can be seen in Figure 1.2.

The easiest parameters to measure are the ones which refer to its ephemeris. That is the times at which an eclipse occurs and the time it takes for everything to happen again. These are, first the epoch or reference moment in time at which the primary (deepest eclipse) occurs in Julian date and then the period in days. These are usually given by the catalogue and are the ones used to find more eclipses and refine the timing of the events.

Firstly let us define the ascending node, this is the point where the orbit crosses the ecliptic curve in the ascending direction, for a non inclined orbit there would be no ascending nodes. From this it follows that the longitude of the ascending node Ω is the angle from a given reference direction to the ascending node itself. Taking this into account we can define the argument of periastron (argument of periapsis in the Figure) ω as the angle from the ascending node to the point of periastron (closest point to the other star) in the direction of orbital motion. In third place we define the true anomaly ν as the angle between lines drawn from the barycenter, to the secondary star, and to the periastron point, where the secondary star comes closest to the primary star.

As for the other orbital and physical parameters we will have to take a more in depth look into the light and radial velocity curves.

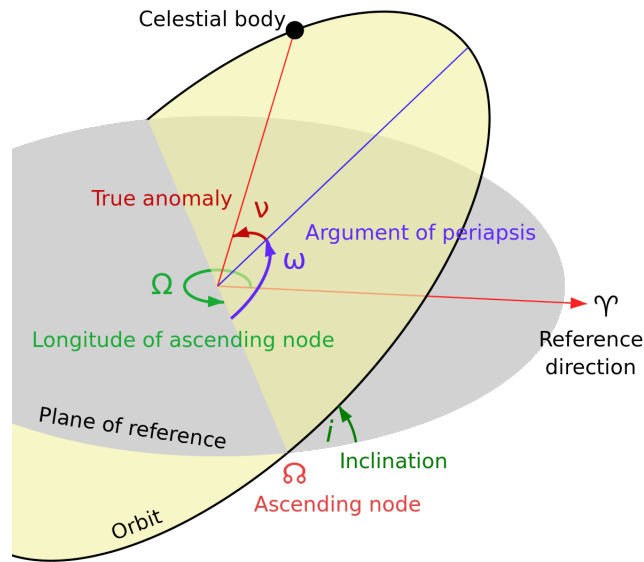


Figure 1.2: Some of the most important orbital parameters. “Diagram of orbital elements, including the argument of periastron (ω).” by Lucas Snyder is licensed under CC BY-SA 3.0.

1.3.1 Light curves

If we were to plot the magnitude or relative flux (the flux of our target star divided by the flux of a comparison star which must not be variable) against time we would see a curve which is flat during most of the orbit¹, 1 and 3 in the previous Figure 1.1, but which has two dips in brightness per orbital period, 2 and 4. The depth, shape and timing of these minima will depend on the types of stars and its characteristics such as temperature, size, luminosity or eccentricity of the orbit. The plot that is obtained is called a lightcurve and its analysis is of great importance because it gives many insights into the different orbital and stellar parameters. From modelling the function that describes the lightcurve we can estimate these values with more precision, in fact this is the reason that makes it an ideal method for studying stars.

All measurements taken in this work are photometric measurements, which in essence is just counting the number of photons which we get from a source. With these measurements we can build lightcurves and then using modelling software we can estimate what the observed stars are like and classify them. Some of the parameters which can be obtained from a lightcurve are the eccentricity of the orbit e , argument of periastron ω , inclination of the orbit i , effective temperatures T_{eff} and luminosity L . We can also give some estimates for the values of the masses but as will be explained in the next section without radial velocity measurements these are just estimates and not real and accurate measurements.

We can expect some constraints on these values, for instance the orbital inclination and eccentricity. First let us take a look at eccentricity, if we have data from many different nights of observation it can be hard to observe the minima and it can appear that we have missed some data. For this reason we can transform from time to orbital phase. This new parameter goes from 0 to 1 and at 0 we would have the primary eclipse and again at 1.

¹This will depend on the proximity of the stars, if they are contact or semidetached binaries this part of the lightcurve called quadrature will not be flat and may be somewhat round.

To do this we would take the Julian date² of observation to which we would then subtract the epoch of the primary obtained from the catalogue and then divide it by the period, lastly the decimal part would be the orbital phase ϕ .

$$\begin{cases} x = \frac{1}{P_0}(\text{HJD} - \text{HJD}_0) \\ \phi = x - [x] \end{cases} \quad (1.1)$$

Where P_0 is the orbital period from the literature, HJD the time in Heliocentric Julian Date at which measurements are made, HJD_0 the central time of primary eclipse in *HJD* format, $[x]$ is the integer part function and ϕ the orbital phase. Going back to the timing of the events, as was previously mentioned the primary eclipse occurs at orbital phase 0. It is obvious that the second one should occur somewhere between 0 and 1. The moment at which the secondary eclipse occurs will directly depend on the eccentricity of the orbit. If we had $e \approx 0$ then the orbit would be circular and the distance between stars would be time independent. In this case the eclipse would occur at $\phi = 0.5$.

From this a question may arise and that is if each star can have different eccentricities. To prove that this cannot be the case let us firstly take a look at the position of the center of mass, which is in the barycenter of the system. This position is given by.

$$\vec{r}_{cm} = \frac{M_1 \vec{r}_1 + M_2 \vec{r}_2}{M_1 + M_2} \quad (1.2)$$

From this equation it follows that.

$$\begin{cases} \vec{r}_1 = \frac{(M_1 + M_2) \vec{r}_{cm} - M_2 \vec{r}_2}{M_1} \\ \vec{r}_2 = \frac{(M_1 + M_2) \vec{r}_{cm} - M_1 \vec{r}_1}{M_2} \end{cases} \quad (1.3)$$

Now let us assume that in Equation 1.2 the frame of reference is at the center of mass, this implies that $\vec{r}_{cm} = 0$ so we would have that.

$$M_1 \vec{r}_1 = -M_2 \vec{r}_2 \Rightarrow M_1 |\vec{r}_1| = M_2 |\vec{r}_2| \quad (1.4)$$

If we define the vector³ \vec{r} such that.

$$\vec{r} = \vec{r}_1 - \vec{r}_2 ; |\vec{r}| = |\vec{r}_1| + |\vec{r}_2| \quad (1.5)$$

²Time should be in heliocentric or barycentric Julian date but we will go into detail as to why later in the next chapters.

³It is not explicitly written but these are all time dependent variables

We can take Equations 1.3 and 1.5 and apply $\vec{r}_{cm} = 0$ to get.

$$\left\{ \begin{array}{l} \vec{r} = \vec{r}_1 - \vec{r}_2 = -\frac{M_1+M_2}{M_1}\vec{r}_2 \\ -\vec{r} = \vec{r}_2 - \vec{r}_1 = -\frac{M_1+M_2}{M_2}\vec{r}_1 \end{array} \right. \quad (1.6)$$

Which substituting by the respective semi major axis and in magnitude would be.

$$\left\{ \begin{array}{l} a_2 = \frac{M_1}{M_1+M_2} a \\ a_1 = \frac{M_2}{M_1+M_2} a \end{array} \right. \quad (1.7)$$

The famous differential equation which describes the orbital motion in a binary system is given by.

$$\ddot{\vec{r}} = -\frac{G(M_1 + M_2)}{r^3} \vec{r} \quad (1.8)$$

A more thorough derivation of this equation and its solution can be seen in the paper by Murray and Correia (2010). The derivation was made for planetary systems but the approximation $M_1 \gg M_2$ was not made so the solution is still valid for this case. The solution for the differential equation is.

$$r(\nu) = \frac{a(1 - e^2)}{1 + e \cos(\nu)} \quad (1.9)$$

Where a is the semi major axis of the elliptical orbit, e the eccentricity and ν the true anomaly angle which was previously defined. To prove that the eccentricities must be the same we should look at Equation 1.5. If we take that the stars

$$r(\alpha) = \frac{a(1 - e^2)}{1 + e \cos(\alpha)} = r_1(\alpha) + r_2(\alpha) = \frac{a_1(1 - e_1^2)}{1 + e_1 \cos(\alpha)} + \frac{a_2(1 - e_2^2)}{1 + e \cos(\alpha)} \quad (1.10)$$

But if we take a similar approach to Equations 1.5 then $a = a_1 + a_2$ so then the previous equation becomes.

$$\frac{a(1 - e^2)}{1 + e \cos(\alpha)} = \frac{a_1(1 - e_1^2)}{1 + e_1 \cos(\alpha)} + \frac{a_2(1 - e_2^2)}{1 + e_2 \cos(\alpha)} \quad (1.11)$$

We can see that that because the relation $a = a_1 + a_2$ is true the the only possibility is that $e = e_1 = e_2$ must be also true. It is known from intuition that the orbital inclination should be in the range of 90° for detached main sequence binaries or otherwise we would not see the eclipse. In general an eclipse will be seen when the following relation is true for a minimum orbital inclination i_{min} , Martínez-Pais (2003).

$$\cos i_{min} = \frac{R_1 + R_2}{a} \quad (1.12)$$

For semi-detached and contact binaries it is easily seen that $R_1 + R_2 \approx a$, however this holds true for detached eclipsing binaries as well.

1.3.2 Radial velocity curves

As previously mentioned there are some parameters such as mass and radius which cannot be accurately measured without radial velocity curves. The question now is what is and how do we obtain a radial velocity curve. In the following paragraphs a brief theoretical deduction of the equations which should be used to determine these parameters will be given, unfortunately no measurements were taken due to a lack of spectroscopical observation.

Let us consider two stars A and B with star A being the more luminous but not necessarily the larger one. If these stars orbit the barycenter of the system and we see them edge on we can expect that one star may be moving toward us and one away from us. As with any other wave emitter it is expected that we will see some Doppler effect on the wavelengths. The light from the star that is coming toward us in its orbital motion will be blueshifted and the light of the star that is moving away from us redshifted. Now if we were to take images of the spectra with a spectroscope we would see that one of the spectra will be moving to the right and another to the left (blue and red shift). If from these images of the spectra we were to mark the positions of the lines for a given time we could calculate the velocity at which they are moving. From the speed at which the lines move we can estimate the velocity at which the stars appear to move with respect to us in the radial direction.

$$v_r(t) = \frac{\Delta\lambda c}{\lambda} \quad (1.13)$$

Where $v_r(t)$ the speed of the star in the radial direction, c is the speed of light in a vacuum, $\Delta\lambda$ the blue or red shift with respect λ which is the non shifted wavelength as it would be measured in a laboratory. If we plot the values of $v_r(t)$ against time we will obtain something like Figure 1.3.

Looking back at Equation 1.4 we can see that.

$$\frac{M_1}{M_2} = \frac{a_2}{a_1} \rightarrow \frac{M_1}{M_2} = \frac{a_2 \sin i}{a_1 \sin i} = \frac{K_2}{K_1}; \quad \left\{ \begin{array}{l} K_1 = a_1 \sin i \\ K_2 = a_2 \sin i \end{array} \right. \quad (1.14)$$

Where K_1 and K_2 are both defined as the semi amplitudes of the radial velocity curves for each component. A general semi amplitude is defined as.

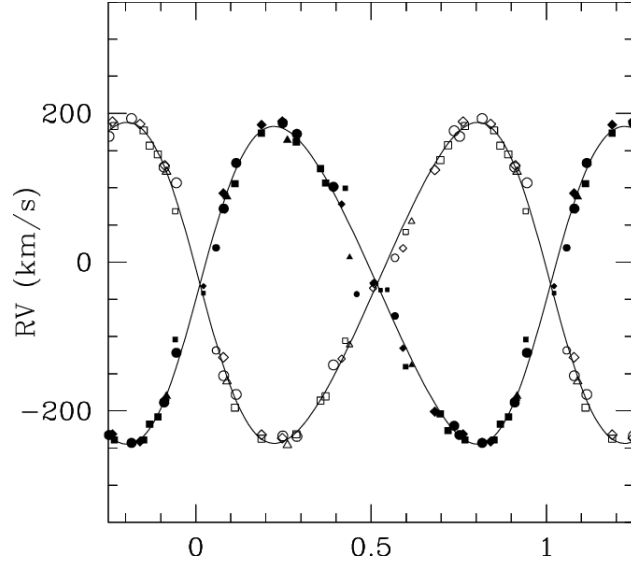


Figure 1.3: Example radial velocity curve of the HD-152248 binary system as computed from the He I λ 4471 line, taken from Sana, Rauw, and Gosset (2001).

$$K = K_1 + K_2 \quad (1.15)$$

If we recall Kepler's third law is.

$$P^2 = \frac{a^3 4\pi^2}{G(M_1 + M_2)} \quad (1.16)$$

Where P is the period and a the semi major axis of the orbit we can fully characterise the masses of each star, if the mass ratio, q , is also known. Now the objective is to combine both Equations 1.16 and 1.14 in some form. To achieve this first we will take the Equation 1.7 and combine it with Kepler's third law.

$$\frac{a_1^3}{a^3} = \frac{M_2^3}{(M_1 + M_2)^3} = \frac{4\pi^2 a_1^3}{P^2 G (M_1 + M_2)} \Rightarrow \frac{M_2^3}{(M_1 + M_2)^2} = \frac{4\pi^2 a_1^3}{P^2 G} \quad (1.17)$$

If now we multiply by $\sin^3 i$ and remember the definition of the semi amplitude of the radial velocity curve, K given by Equation 1.14 we have that.

$$\left\{ \begin{array}{l} M_2^3 \sin^3 i = \frac{(M_1 + M_2)^2 4\pi^2 a_1^3 \sin^3 i}{P^2 G} = \frac{((M_1 + M_2) a_1 \sin i)^2 4\pi^2 a_1 \sin i}{P^2 G} \\ M_1^3 \sin^3 i = \frac{(M_1 + M_2)^2 4\pi^2 a_2^3 \sin^3 i}{P^2 G} = \frac{((M_1 + M_2) a_2 \sin i)^2 4\pi^2 a_2 \sin i}{P^2 G} \end{array} \right. \quad (1.18)$$

Using again the Equations 1.7 we finally get.

$$\left\{ \begin{array}{l} M_1 = \frac{4\pi^2 K_2 K^2}{P^2 G \sin^3 i} \\ M_2 = \frac{4\pi^2 K_1 K^2}{P^2 G \sin^3 i} \end{array} \right. \quad (1.19)$$

From this equation we can calculate the masses if we know the orbital inclination, period and most importantly the semi amplitudes of the radial velocity curves.

1.4 Different types of eclipsing binaries

There are various ways of classifying binary star systems, one of them is by the shape of the lightcurve produced by the eclipses which will be the one discussed in this section. Example lightcurves can be seen in Figure 1.4.

1.4.1 Algol type

Algol type eclipsing binaries are characterised by the separation between the two components, they are detached from one another. These stars lightcurve's are mostly flat outside of the eclipses as the one in Figure 1.1 and may present two different eclipses. In most cases there is no matter exchange but in some cases it does occur in the form of direct accretion and in extreme cases and accretion disk as is the case for W Serpentis stars. It is not uncommon for each star to be of different spectral type and thus of different brightness. In these cases one can expect that each eclipse has a different depth. The deeper or primary eclipse occurs when the colder star passes in front of the hotter one and reversely for the secondary eclipse. In general this may not mean that the star that is behind is smaller or larger, only that it is less superficially bright than the other one.

1.4.2 Beta Lyrae

This is a type of binary (and in the scope of this work also eclipsing) that is characterised by a distortion of the star's shape. These stars are ellipsoidal in shape due to the gravitational action of the companion. In general they need not exchange mass may only feel each other's presence through gravity and radiation. However depending the evolutionary state of each component mass exchange can happen. Mass accretion from one star to another will occur when the first one's radius grows larger than its Roche lobe. The Roche Lobe is a volume around a star which is defined as the regions created when the critical equipotential surface crosses itself in a geometric saddle point, see Peter Eggleton's definition, Eggleton (2006), basically the region around a star where matter is gravitationally bound. This equipotential surface is defined by the amount of mass in the system so if one of the stars begins to increase in radius, for example if it is in a later evolutionary state than the companion, and the volume it occupies gets larger than the Roche Lobe that surrounds it, it can begin to accrete mass to its companion. The mass will go to the the "inner Lagrangian point" and from there fall into the companions gravitational influence. The effects this has on

the lightcurve are noticeable. Because of the tear-drop shape of these stars although they are separated the lightcurve does not present the usual flat out of eclipse part and is somewhat rounded.

1.4.3 W Ursae Majoris

These are binary systems where both components have exceeded their Roche Lobe and are physically in contact with one another. They have a short orbital period and share mass and energy through the joint part. Because of this reason they usually have the same temperature and the depth of the minima is similar. As for the lightcurve it is sinusoidal in shape.

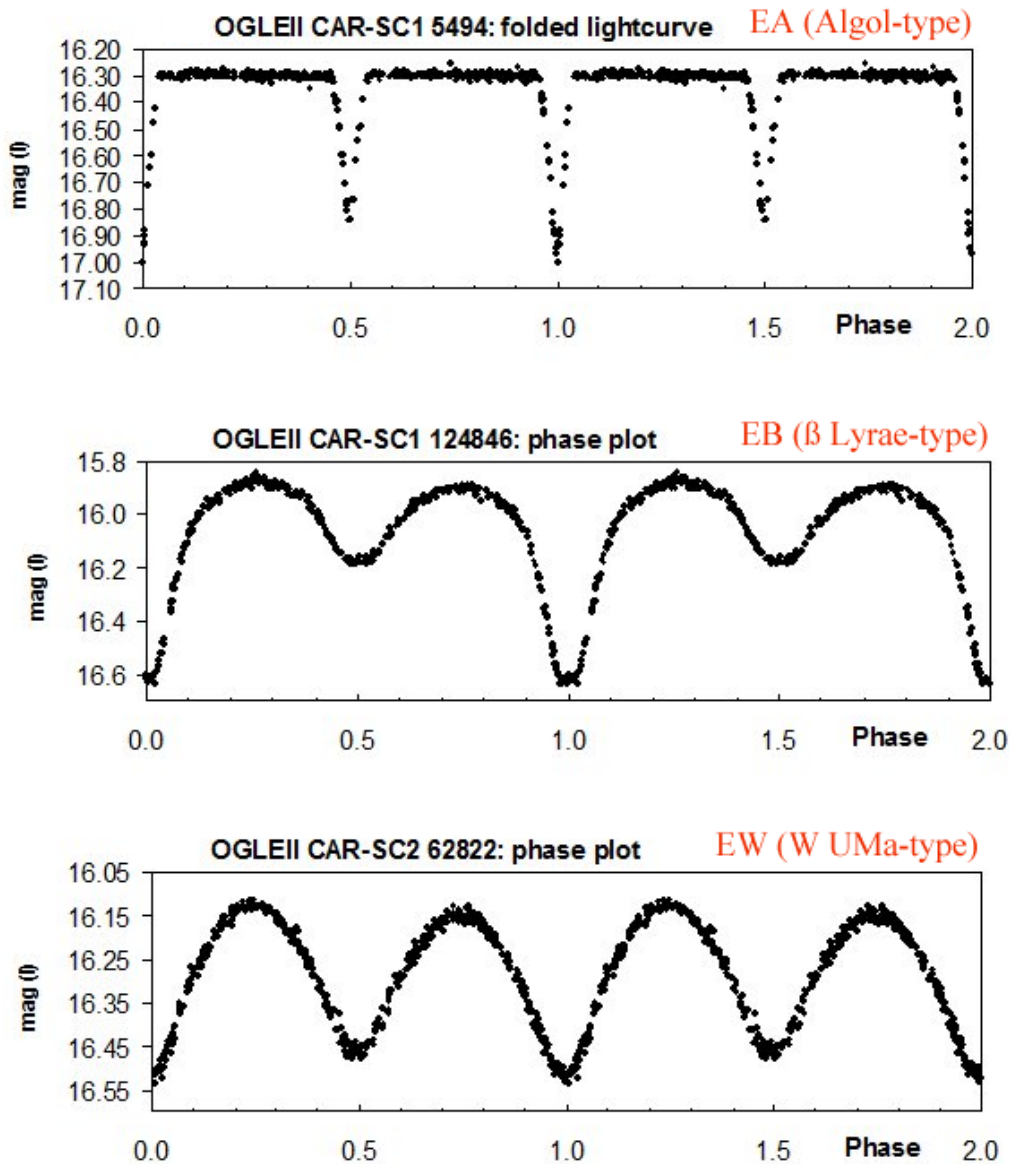


Figure 1.4: Different spectral type lightcurves, Huemmerich and Bernhard (2012)

Chapter 2

Observations and data reduction

En este capítulo se exponen los motivos por los que se eligieron las dos estrellas estudiadas en este trabajo, los telescopios e instrumentación usados, reducción de datos y fotometría.

2.1 Observations

From the previous chapter the scientific case for studying binary stars is now clear and after understanding the underlying physics one should decide what observations to make. Deciding what can be observed can be daunting and will depend on the facilities one has access to. For example if the target is too faint it will require to be observed with a larger telescope. For this work two targets were selected. These targets were observed each with a different telescope and had to fulfill a number of prerequisites.

2.1.1 ASASSN-VJ050229.84-052203.4

The first target that was selected was ASASSN-VJ050229.84-052203.4, ASAS05 from now on. The target was selected for various reasons. First of all it could be observed in late 2022 and early 2023. This is important because that way if there were any issues with the target such as an unresolved companion or any other issues this could be spotted early and accounted for. Besides it is also helpful to have the data some time before having to reduce it analyse and to not be in a rush. To know if it would be observable one would have to look at its altitude curve. This altitude curve, Figure 2.1, gives information about the object visibility throughout the night and allows for planning taking into account telescope limits and minimum moon separation.

Secondly the target has not been in publications, it is in catalogues and in the corresponding data release papers but no individual paper has been dedicated to this target. This is a bonus because these are the first proper dedicated studies of this object.

Thirdly it has a period which allows for good temporal sampling. For this science case the period should not be too long as we would not be able to fully cover the quadrature, too short because the transit duration would also be short and therefore we would not be able to reliably measure it and finally close to one as in that case we would mostly see the same thing every night. Ideally the target should be in the 0.7 to 0.8d range which this one is.

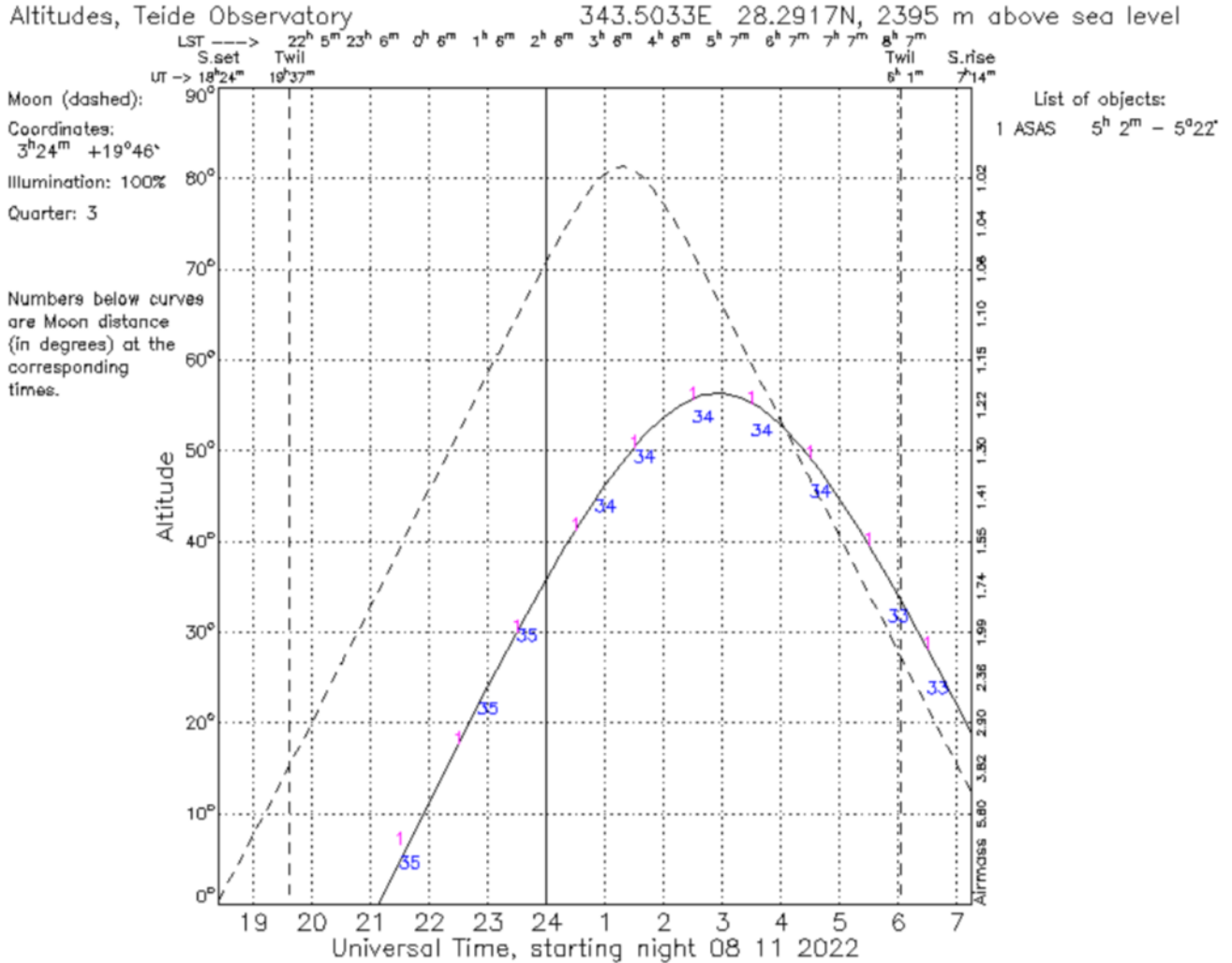


Figure 2.1: Altitude curve for ASAS05 as of 08/11/2022, plotted using STARALT, developed for the Isaac Newton Group of Telescopes by Peter Sorensen, Marco Azzaro, Javier Méndez.

Fourthly the magnitude should be enough to be seen by the telescope. If the magnitude is too low it would require a longer integration time which would compromise the certainty of the temporal sampling during eclipses if they are too short. ASAS05 was selected from the ASAS catalogue number 2, Jayasinghe et al. (2018), and was observed with the IAC80 telescope at Observatorio del Teide, OT for short. It was observed on 08/11/22, 03/12/22, 15/12/22 and 08/02/23 in the Johnson *V*, *R* and *I* filters with exposure times 300, 200 and 150 s all nights except on the 03/12/22 where it was 150, 100, 100 s with the telescope focused. In general it is preferable to have longer exposure times in the bluer filter given the scattering that occurs in the atmosphere. An example of the field around the star can be seen in Figure 2.2

2.1.2 CRTSJ041918.8-071807

In this case the target, CRTSJ04 from now on, was taken from the CRTS catalogue, Drake et al. (2011). This target is much more interesting than the previous one from a scientific standpoint, that is because this is a very short period (0.22d) M dwarf binary.



Figure 2.2: Centered field of view around ASAS05; taken from the ALADIN lite service, Boch and Fernique (2013), Bonnarel et al. (2000). The target can be seen marked by the purple cross and the comparison star by the red circle.

This target completes an orbital period in roughly 5 hours and both stars seem to be at least semidetached from preliminary results Papageorgiou et al. (2018). It also fulfills all the prerequisites specified in the previous section so it is an ideal target to study which was observed with the Carlos Sanchez telescope at OT. The target was observed on the nights 02/11/22, 11/11/22 and 13/01/23 with exposure times of 15, 40, 40, 40 in the first night, 60, 60, 60, 15 in the second, 120, 100, 60, 15 s in the last night¹ in the Sloan g' , r' , i' and z'_s filters. Once again the field can be seen in Figure 2.3

Finally, in the next table the main identifiers and general parameters for both targets can be found.

	ASAS05	CRTS04
TIC	213068982	67858869
Right Ascension (J2000)	$05^h 02^m 29.84^s$	$04^h 19^m 18.8^s$
Declination (J2000)	$-05^\circ 22' 03.4''$	$-07^\circ 18' 07''$
$Vmag$	13.87	17.80
Epoch [HJD]	2457359.86888	2459886.51565
Period [d]	0.7672625	0.2221148
Telescope	IAC80	TCS

Table 2.1: Main parameters of the two targets, the first line being the TESS Input Catalogue id number.

¹The reason for the 15 second exposure times will be given in the TCS-MuSCAT2 section

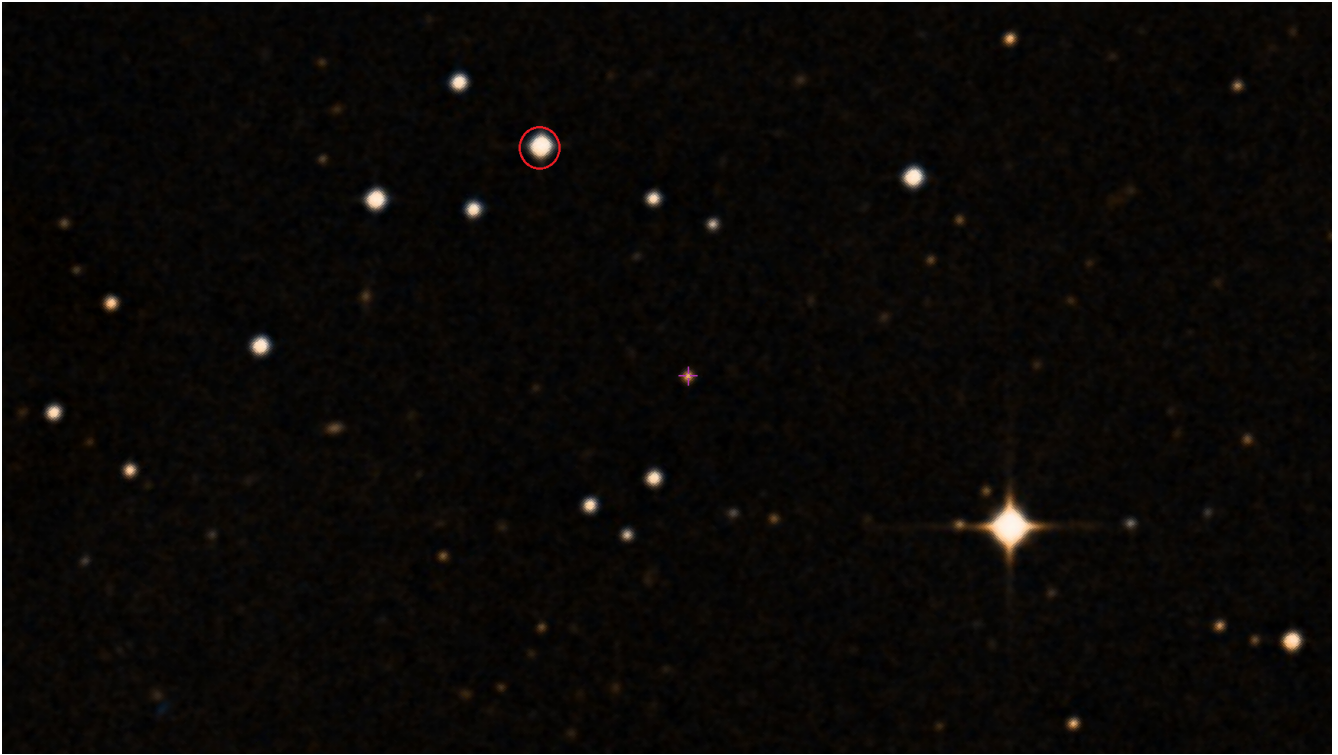


Figure 2.3: Centered field of view around CRTS04191; taken from the ALADIN lite service, Boch and Fernique (2013), Bonnarel et al. (2000). The target can be seen marked by the purple cross and the comparison star by the red circle.

2.2 Telescopes and instruments

Two telescopes were used in the observations as previously mentioned. This is because each telescope is best suited to a certain type of science, it will now be explained.

2.2.1 IAC80 - CAMELOT2

The IAC80 telescope was the first telescope developed entirely at IAC. Development began in the 1980s and it was installed at OT in 1991 where it began to operate in 1993. It is a classic Cassegrain telescope with a primary mirror of 82 cm and effective focal length of 9.2 m. It is mounted on a German Equatorial Mount designed to accommodate multiple instrumentation. The instrument used was CAMELOT2 (CAmara MEjorada LIgera del Observatorio del Teide) which has a 4096x4096 pixel CCD, which stands for Charge Coupled Device, 21.98'x22.06', and 15x15 micron pixel size and a plate scale of 0.322"/px. Unfortunately the filter wheel is smaller than the field of the CCD so there is some vignetting so the real field of view, FOV, is around 11.8'x11.8'.

The camera verifies linearity up to 56000 ADU, where ADU stands for Analog to Digital Unit, and has a quantum efficiency of 90% at 700 nm. It is cooled down to -104.5°C with a vacuum chamber (Prieto (2004) this is for the old camera CAMELOT but the new one is very similar in this regard) so the dark current effect is negligible and no dark calibration images are required. All flats were dome flats and there are 11 of them per filter with 21 bias frames as well. This telescope is well suited to the ASAS target given its magnitude and the fact that the transit duration is long enough to have good temporal sampling. If the

transit duration were shorter it would be a problem because there is some time lost every exposure due to filter change and readout time which both are in the 10 seconds range.

2.2.2 TCS - MuSCAT2

The Carlos Sanchez telescope is a Dall–Kirkham Cassegrain telescope with a 1.52m aperture which first started service in 1972. It is specialised in infrared astronomy which suits the target in question. That is because M dwarfs are very faint stars with a low effective temperature and which primarily emit in the infrared range. The main instrument installed at TCS is MuSCAT2. This is an instrument developed by the Astrobiology Center (ABC) and the University of Tokyo (UT), in collaboration with the Instituto de Astrofísica de Canarias (IAC). It allows for simultaneous photometry in four filters by making use of 3 dichroics that split the light which each go to the respective CCD, Narita et al. (2018). The CCDs have a FOV of $7.4' \times 7.4'$ with $0.435''/\text{px}$. The cameras are cooled to -70°C and in this case there are dark calibration frames.

2.3 Data correction

Due to logistical reasons the telescope cannot be cleaned everyday as it would require the mirror to be removed each day and that is not possible. Because of this reason there may be some dust buildup in the mirrors or other surfaces. This is only one of the possible many sources of error when taking images. This is a problem because if these errors are not accounted for one could think that for example the magnitude of a star is much lower than what it really is. There are of course other intrinsic effects to the CCD such as The way to correct the science images is by taking other calibration images. There are a number of these images and each of them serves a different purpose.

2.3.1 Bias

There are three main sources of noise the first one being readout noise. The bias is an artificial offset added to the data to avoid negative values in the signal due to the readout noise, for example in an ideal case the sky would be dark so the signal in that region should be zero but because there is some readout noise the sky value may be negative. Back when computer storage capacity was an issue wasting bits in coding negative values was considered a waste so this artificial offset was introduced. The proper way to correct the image of bias is to take 21 images with 0s exposure time, i.e. shutter closed, mirror covers closed and, if one wants to be extra sure that there is no signal, with a narrow band filter as well.

2.3.2 Flat-Fields

Due to many different reasons, for example dust buildup or different response to light of each pixel, if we had two perfectly equal stars whose light travels through the same part of the sky we would not see them perfectly equal when imaging them. This is because the CCD sees differences in illumination in each part of the field of view. This difference is pixel and filter dependant. The correct way to take these calibration frames is to point at a evenly illuminated surface with around 30000ADU and to take the usual 11 frames per filter. These evenly illuminated surfaces could be a screen inside the dome which is lit by lights or ideally a part of the sky with not many stars just before and after twilight.

2.3.3 Darks

There is one other effect called dark current. When taking long exposure images the internal circuits of the camera get hot by Joule's first law. When this happens there is some thermal photon emission so the CCD receives these photons and sees an artificially illuminated frame. There are two ways to eliminate this dark current effect, firstly by cooling the camera well below zero and secondly by taking dark calibration images. Because thermal emission occurs primarily in the infrared it is specially important to take into account in telescopes which observe in this wavelength range as is the case of TCS. In the case of IAC80 this effect is mostly negligible because of the temperature to which the CCD is cooled. To take dark frames one would cover the mirrors and then take images with no filter with the same exposure times as in the science images. Finally there is also a subset of dark frames taken to specifically correct the flat frames called dark flats, these are done with the same exposure time as in the case of the flats.

2.3.4 Image correction

The first step that was taken was to crop the fits files due to the vignetting previously mentioned. Then if we assume the image signal is given by.

$$S(x, y) = B(x, y) + (O(x, y)F(x, y) + D(x, y))t_{exp} \quad (2.1)$$

Where S is the signal as provided by the CCD, B is the bias signal, F the flat-field signal and D the dark signal and O the original non altered signal. Let us assume a $t_{exp} = 1 \text{ unit}$ for simplicity. Then the original signal would be related to S by.

$$O(x, y) = \frac{S(x, y) - B(x, y) - D(x, y)}{F(x, y)} \quad (2.2)$$

So finally one would have to create a masterbias frame by averaging all bias frames. Then subtract this image to all other including the rest of calibration frames. For the flat-fields one would subtract the masterdark frame if there are any and then average all flats into a masterflatfield which is the normalised to one. Finally the corrected signal would be given by Equation 2.2 where it is important to note that every value in the right hand side except S is a master frame. A brief schematic image representative of the process can be found in Figure 2.4

2.4 Photometry

Once all images have been calibrated one can begin doing science on them. All steps described in the following two sections will refer to the work performed on the IAC80 observations as in the TCS case everything is automated via the pipeline which uses PyTransit developed by Hannu Parviainen and described in Parviainen 2015. For the purpose of automation a pipeline has been constructed. This pipeline will, with little user input, take care of all the tasks necessary to provide the flux of a star². The first step is to locate where the target is and which comparison stars to use in order to measure the relative flux or magnitude.

²The calibration process and other functionalities such as astrometrisation are also automatically done via the pipeline.

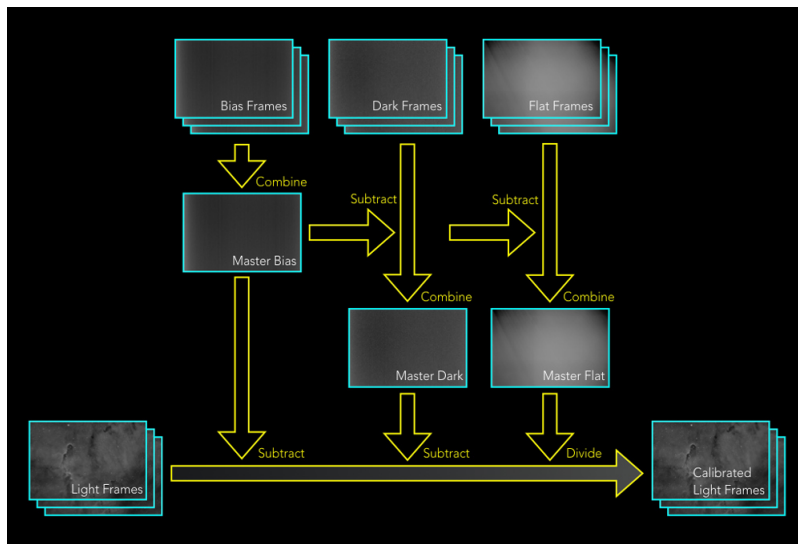


Figure 2.4: Calibration process. “Subframe calibration processing flow.” by Peter Hergesheimer is licensed under CC BY-SA 3.0.

2.4.1 Astrometry

One of the easiest ways to know where the stars are is to manually look at the field of view in ds9 and compare it to the one that could be seen in a tool such as Aladin lite. Then align all images to a reference frame and continue performing photometry. However this is not ideal if there are multiple nights of observation as the field of view may not be the same each night and different stars will be included each night. This is the case in the observations made with IAC80. One way to workaroud this, which is in fact preferable in most cases, is to astrometrise. Astrometry is a technique in which the positions of celestial bodies in pixel and sky coordinates obtained are related via a transformation function. Also astrometrisation allows for target selection. In this pipeline a functionality has been included in which a ds9 window opens up with all recognised stars marked by order of brightness. The user can then select which stars to do photometry on, then the pixel coordinates are transformed to Right Ascension, RA, and Declination, Dec, and after that these coordinates are used for all other frames.

Astrometry was performed on all images using Astrometry.net API for python, Lang et al. (2010). Astrometry.net takes as input a list of star positions in pixel coordinates which represent the centroid of the stars found using Daofind from IRAF/PyRAF or DaoStarFinder from photutils. Then it compares the patterns that the star form with those found in popular catalogues such as 2MASS, Skrutskie et al. (2006), and GAIA Brown et al. (2021). After a solution has been found Astrometry.net returns an Astropy WCS (world coordinate system) header. This is a header which contains the coordinate transformation function from pixel position to right ascension and declination. One can update each fits file with this new WCS header and then use it for future coordinate transformations without the need to generate new files. Astrometrisation is a very useful tool when doing photometry. If the target and comparison star’s coordinates are known then one can simply access the WCS transformation found in each updated fits file and using that function get the pixel position of the stars in each image.

2.4.2 Aperture photometry with PyRAF and PhotUtils

The first step when doing photometry is to select the target and comparison stars. For this case it is interesting to select a “standard”. A standard in this case does not refer to the usual meaning such as in the Landolt standards, Landolt (1992), but comparison star which has been studied or catalogued and with magnitudes which are well established for different filters. The reason behind this is that in this way one can eliminate the atmospheric extinction effect³ without having to calculate the extinction coefficient k . The comparison star selected is the Tycho-2-4758-615-1 of $Vmag = 11.590$ found in the Tycho-2 main catalogue, Hog et al. (2000).

There are two main python modules with which to perform aperture photometry. PyRAF is a command language based on python for the original IRAF (Image Reduction and Analysis Facility) originally maintained by the NOAO (National Optical Astronomy Observatory) to perform various image reduction and astrophysical tasks. On the other hand Photutils is “an affiliated package of Astropy that primarily provides tools for detecting and performing photometry of astronomical sources”. Pyraf’s main advantage is the ease of use and in fact was mainly used in the image correction process, there are however a number of drawbacks. Firstly it generates many files which unless deleted may bring up file errors in the code. The second and most important reason is that the aperture photometry done with photutils yields slightly better results specially when dealing with smaller apertures, Bajaj and Khandrika (2017)).

To perform aperture photometry with this package there are a number of easy steps to follow. First the aperture radius should be defined. The aperture defines the area over which the number of ADUs will be counted, from this it will be possible to estimate the instrumental flux of the star. In general the aperture should be large enough to accommodate the whole star but not so large that the light of other gets blended with the target’s light. The standard is to have an aperture of 1.5 to 2 times the size of the full width at half maximum of the point spread function. The PSF will be determined by the seeing. The seeing is defined in arcseconds and is a measurement of the turbulence of the sky and determines, in most cases⁴, the absolute best resolution a telescope can achieve.

The area selected however, does contain some background level which is given by the sky illumination. To subtract this background level a part of the sky must be measured. To achieve this we add a bigger circular corona around the PSF, this circular corona has an inner radius, annulus, that should be at least the same size as the aperture and a outer radius, dannulus. The annulus should be around 4 times the FWHM of the star’s profiles and the dannulus should be between 2 and 5 pixels larger. The size difference between the two should not be too big because the area of interest is the local sky around the star.

Aperture photometry can be performed with the following PhotUtils function *aperture_photometry(data, aperture, error)*. Where data is the fits file on which to perform photometry, aperture the circular aperture sum to which the background level will then be subtracted, and the error refers to the background and Poisson error which should be previously estimated. To calculate this error one could look at the *calc_total_error(data, sky_sigma, gain)* functions, where *sky_sigma* is the standard deviation of the sky in counts with a maximum of 3σ , this will include both the sky induced error as well as the Poisson error due to the bright sources.

³Ideally this would not be the case, but due to bad weather and lack of photometric nights no calibration with standard stars could be done, however the magnitudes of the comparison star used for ASAS05 are established well enough to do this.

⁴For telescopes with adaptive optics systems or an aperture of less than 20 cm in good observatories the best resolution will be given by the aperture of the telescope.

After this has been done the total error will be given by.

$$\text{error} = \sqrt{\sum \sigma_{tot}^2} \quad (2.3)$$

Where σ_{tot}^2 is the total error calculated by the *calc_total_error* function. After these steps the instrumental flux and instrumental error have been calculated. Now it would be interesting to go from instrumental flux to instrumental magnitude and from there to real apparent magnitude. With the apparent magnitude one can estimate the spectral type of the stars. To transform from instrumental flux to instrumental magnitude mag_{ins} the IRAF phot equation from the daophot package has been used.

$$\text{mag}_{ins} = \text{zmag} - 2.5 \log_{10}(\text{flux}) + 2.5 \log_{10}(t_{exp}) \quad (2.4)$$

Where *zmag* is the zero point magnitude, an arbitrary zero magnitude which was set to 25. The error is given by.

$$\text{error} = \sqrt{\text{flux}/\text{gain} + \text{area}_{aper} \sigma_{sky}^2 (1 + \text{area}_{aper}/\text{area}_{annulus})} \quad (2.5)$$

Obtaining the following results for the comparison star, see Table 2.2.

Filter	Catalogue Magnitude	Mean Instrumental Magnitude
V	11.590	18.3530 ± 0.0010
R	11.117	18.6990 ± 0.0010
I	11.040	18.9330 ± 0.0006

Table 2.2: Second column contains the magnitudes for the Tycho-2-4758-615-1 comparison star, the V magnitude was taken from the Tycho-2 main catalogue Hog et al. (2000), and the rest from the NOMAD catalogue, Zacharias et al. (2005). All of them accessed via the Vizier service, Ochsenein, Bauer, and Marcout (2000). The third column, mean instrumental magnitude, is the magnitude of the comparison star as experimentally measured with a linear offset from the assumed true magnitude given in the second column.

From Table 2.2 by subtracting the second and third columns we can estimate how much of an offset there is between the instrumental magnitude and the real magnitude. Finally the following results have been obtained for the magnitude of the ASAS05 star, they can be found in Table 2.3.

Filter	Out of Transit	Primary	Secondary
<i>V</i>	14.0150 ± 0.0030	14.6005 ± 0.018	14.0598 ± 0.0031
<i>R</i>	13.8548 ± 0.0031	14.4171 ± 0.018	13.9241 ± 0.0032
<i>I</i>	13.4910 ± 0.0028	14.0310 ± 0.018	13.6510 ± 0.0027
<i>V – R</i> Primary	<i>V – I</i> Primary	<i>V – R</i> Secondary	<i>V – I</i> Secondary
0.19	0.57	0.13	0.4

Table 2.3: Mean magnitudes for ASAS05 calibrated using the “standard” comparison star. Also included in this table are the colour differences for different filters.

The results obtained from the colour differences, Johnson (1966) and Pecaut and Mamajek (2013), from the NOMAD catalogue are compatible with the colour information of the binary presented in this work. These suggest that the primary star is an A7. As for the secondary star no conclusive result can be given because in this case the primary star still contributes some amount of flux making the secondary component apparently bright. This is also compatible with the T_{eff} that can be found in the Gaia database. The obtained lightcurves can be seen in Figure 2.5.

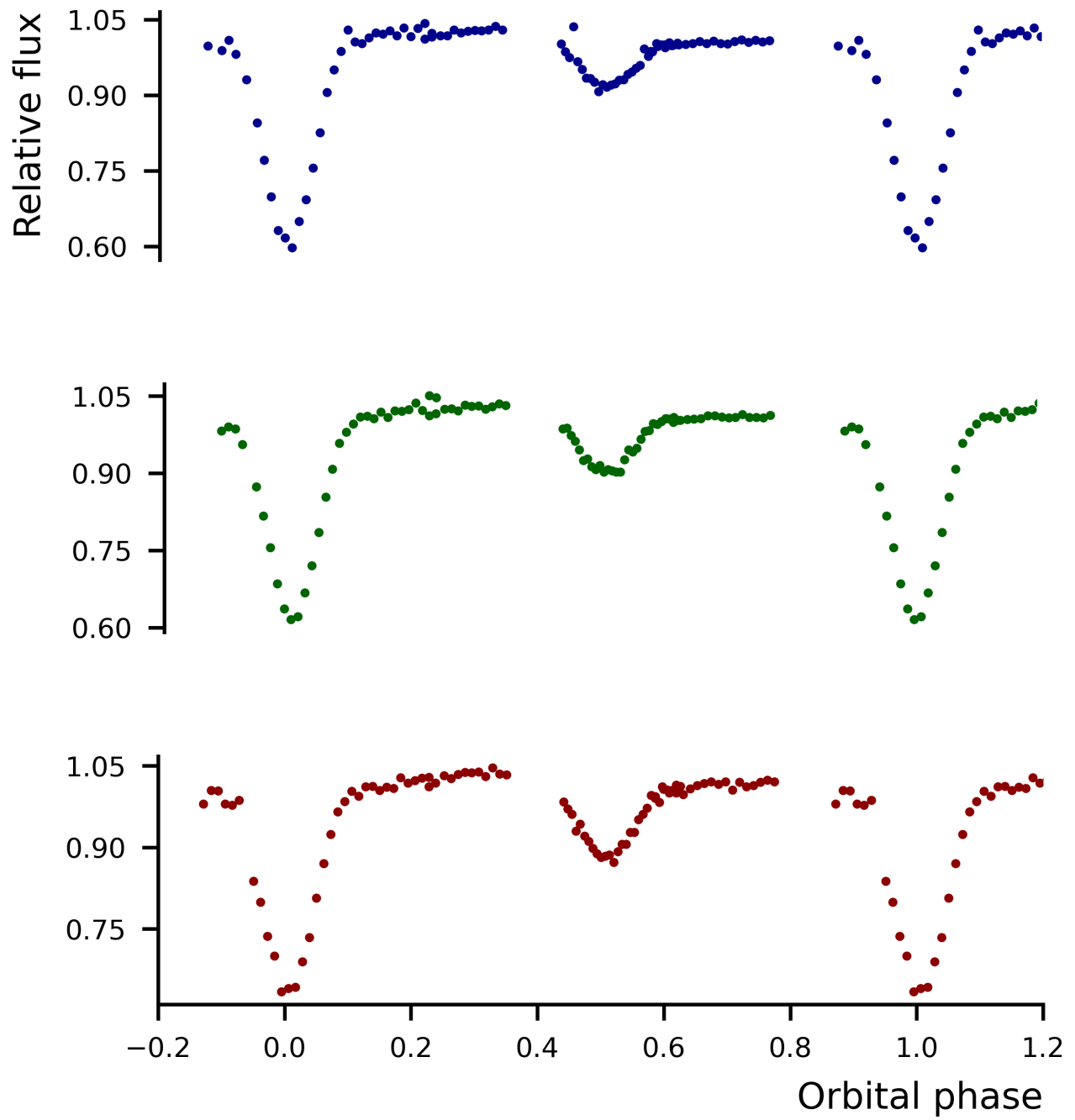


Figure 2.5: ASAS05 normalised relative flux lightcurve, filters are V, R, I from top to bottom.

Regarding CRTS04 the process is much different. The pipeline utilised makes use of the previously mentioned python module PyTransit Parviainen 2015 which is extensively documented. The calibration of bias, flat-fields, darks and dark flat-fields are performed automatically after each night of observation. In this case darks are quite important given that the CCDs have a non negligible dark current.

The transit analysis is performed via Jupyter Notebooks where the code is run, one is created for each target and night. In this notebook the target and comparison stars are selected. If there are any outliers in the data or or large systematics at some times these can be eliminated (for example if there was dome vignetting). After that some prior values were given for the period, P and time of superior conjunction, T_0 taken from the literature, Papageorgiou et al. (2018), the program was set to find the best combination of apertures and comparison stars for 30,000 iterations.

Finally some posterior distributions are sampled using 5000 MonteCarlo iterations and from this the uncertainty in fluxes is obtained. Because MuSCAT2's pipeline is primarily designed for exoplanets, it only produces normalised relative flux, which is good for visualization purposes but you loose information regarding magnitudes and other phenomena such as possible stellar spots. Given this impossibility to obtain proper magnitudes from the data we referred to the NOMAD catalogue to check for the magnitudes in different filter and from there obtain the colour difference. This will serve for a preliminary stellar classification of the stars, similarly to what was done in Table 2.3. The results obtained in Table 2.4 suggest that the primary star is in the K7 to M2 range, Pecaut and Mamajek (2013).

B	V	R	J	H	K
18.35	17.800	16.690	14.432	13.773	13.507
B-V	V-R	V-J	V-H	V-K	
0.19	0.57	0.13	0.4		

Table 2.4: Mean magnitudes for CRTS04 from the NOMAD catalogue, Zacharias et al. (2005). Also included in this table are the colour differences.

The lightcurve can be seen in Figure 2.6. Both stars are M dwarfs so it was expected that in the shorter wavelengths where they emit less light the scatter in the lightcurve would more significant.

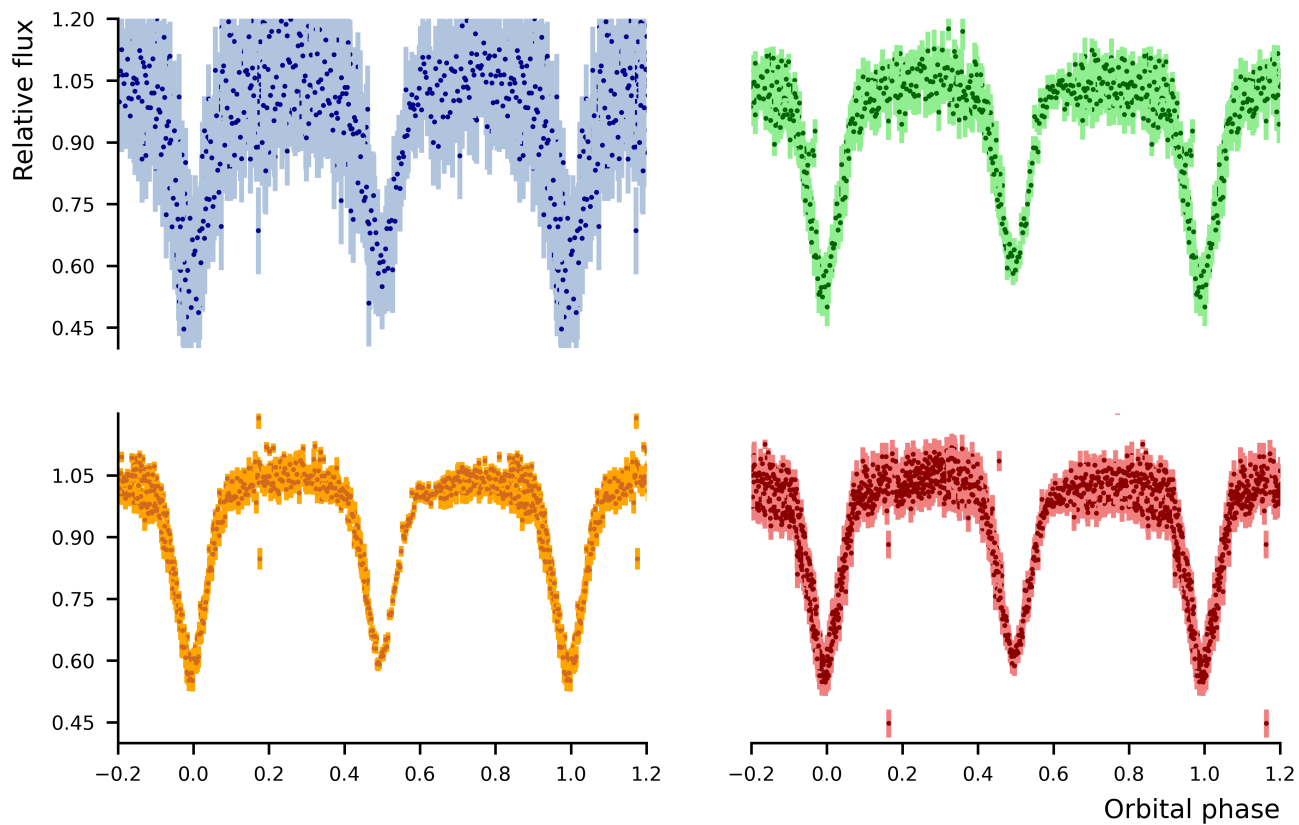


Figure 2.6: CRTS04 normalised relative flux lightcurve, filters are g' , r' , i' and z'_s from left to right and top to bottom.

Chapter 3

Lightcurve modelling

En este capítulo se describirán los métodos utilizados para hacer un ajuste de una curva de luz. Se describirán los resultados obtenidos y se darán nociones de los pasos más avanzados como uso de algoritmos Monte Carlo para la estimación de incertidumbres.

3.1 PHOEBE2

PHOEBE2, PHysics Of Eclipsing BinariEs, is a python package with sophisticated modelling capabilities for all eclipsing binary observables mainly radial velocity and light curves as well as spectral line profiles though there are other planned functionalities yet to be released.

The usual working flow in PHOEBE consists in a series of steps listed in Figure 3.1.

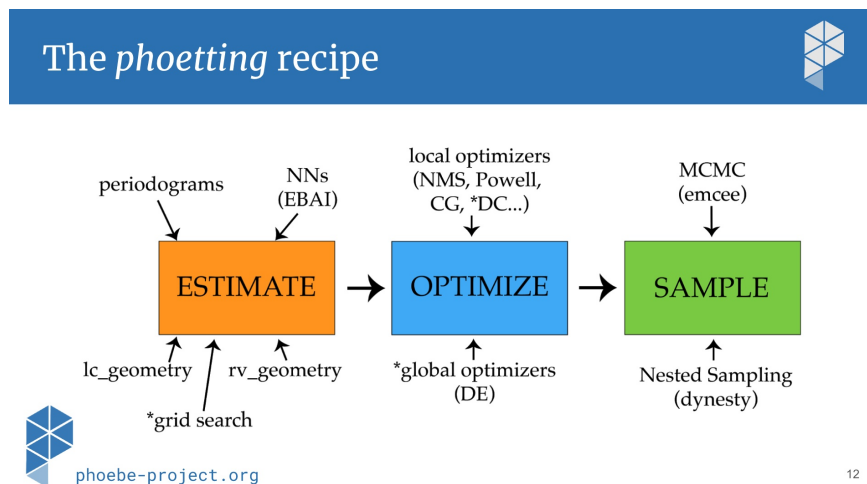


Figure 3.1: PHOEBE workflow. Image taken from Angela Kochoska’s talk on the inverse problem during the June-July 2022, Villanova PA PHOEBE 2 workshop.

In general the first step is to estimate parameters that somewhat fit the lightcurve. Given Gaia’s mission success we will assume a number of parameters for the model. For instance one would set as constraints, that is fixed values, the ones which one has some idea of what they might be, for example temperature ratio. The program takes this values and from these constraints tries to fit some new parameters which are derived from the first ones.

This will most likely not be the most accurate and serve only as estimators which will then be input in the next step.

Step two consists in using different optimizing algorithms to find the best fit curve to the data. In this part one will “flip” constraints to variables as needed in order to obtain an accurate model. In general this is a very manual and time consuming process and in most cases it is also very computationally costly as PHOEBE, although very robust, consumes a lot of resources from the computer or server it uses to run. This is one of the main reason why the lightcurve models presented in this work are not the final ones and have room for improvement.

Finally in the last step one would create posterior distributions to calculate the most likely errors in the fit parameters using Markov Chain Monte Carlo (MCMC) algorithms or some other. This, once again, is very computationally costly and has not been done in this work.

3.2 Lightcurve modelling of ASAS05 and CRTS04 stars

PHOEBE2, Prša et al. (2016), is a new and improved version of the original PHOEBE code which was mainly based on the renowned Wilson and Devinney (1971), WD from now on. The WD code assumes that binaries are in synchronous orbits and that they follow the Roche model geometry explained in the first chapter. The model creates a surface representative of the star’s Roche lobe called mesh (originally made up of trapezoids) where the flux is discretised into each mesh point. This discretisation allows for a somewhat easy computation of the physical phenomena, for instance limb darkening (the darkening of the star around the edges of the stellar disk) and shapes due to tidal forces among others, and intrinsic parameters of the stars like the radii. The model calculates the star’s brightness in order to create a model lightcurve which it then compares to the real lightcurve. The model tries to minimize the differences between the two by iteratively changing the fitting parameters (radius, temperature and others) and using an optimizing algorithm such as the one developed by Nelder and Mead (1965) to get to the most likely solution. However one of the many problems with this is that a wrong combination of parameters can provide a good geometric solution to the lightcurve.

For this reason Prša and collaborators developed PHOEBE2. In this program the trapezoidal mesh is replaced by a triangular one which avoids disconnection between different mesh points. This is extremely useful in most cases but specially useful when modelling accretion disks, contact binaries or even other more outlandish phenomena according to Prša.

3.2.1 ASAS05

The first step is to initialise a model by starting a phoebe bundle and adding a dataset. To add a dataset one must specify the time of observation, for instance Barycentric Julian Date, provide the fluxes and uncertainties all as python arrays. Other secondary options include specifying the filter used or pass-band luminosity. After that has been done the preliminary physical parameters can be set. In order of implementation they were atmosphere mode which was set to a black body approximation and then limb darkening which was set to follow a logarithmic function. Once that has been done an estimator forward model can be initialised. There are many of them but two produced exceptionally good results. They both use Artificial Intelligence models to fit a model to the data. The first one is called EBAI (Eclipsing Binary Artificial Intelligence) KNN which uses trained python’s scikit learn.neighbors.kNeighborsRegressor

model to fit the data and the second one called EBAI MLP which uses a trained neural network. In the case of ASAS05 an EBAI MLP model was used. The best fit model can be seen in Figure 3.2. For this model the temperature of the primary was set to be 7299K which is the T_{eff} that can be found in the Gaia's data release 3, Brown et al. (2021). The temperature of the primary was set to this value because given that the star is an A type and that Gaia primarily observes in the optical range the light of the primary will dominate over the light of the secondary star, a G type. Besides the temperature of A stars is around the 7000K range.

3.2.2 CRTS04

A very similar workflow was followed for CRTS04, however in this case an EBAI KNN model was used, the reason behind this is that the EBAI MLP model fails to converge when the amplitude of the eclipse is too big for the method, more precisely when the amplitude of the eclipse is more than 0.20 in phase. The primary temperature prior was set to 3387K, again from the Gaia database for this target. The parameters set as variables in the model were the eccentricity, time of superior conjunction and temperature of the secondary. The lightcurve model for this star is in Figure 3.3.

3.2.3 Nelder-Mead optimization

Finally as a tentative first step in optimization some fitting was carried out. The optimization model used was Nelder-Mead, in essence the model takes the previous fitted parameters and tries to further optimize them, though the results were not optimal due to time and hardware limitations. For this simple optimization 150 iterations per filter were performed with a total computational time of 15-20 minutes per filter. From this one can see that effectively PHOEBE2 is very computationally expensive and in fact, as can be seen in Figure 3.4 the optimization did not have time to fully converge and provide an accurate solution, the primary eclipse depth is not correct and the trends in the residuals plot are quite strong. From the PHOEBE2 documentation it is stated that running PHOEBE2 in a server with 72 cores it can take up to 2 hours for an optimal solution to converge. The computer used for this work has 8 cores so the time needed for a convergence would be unfeasibly long. The result obtained for the R filter lightcurve of ASAS05 is in Figure 3.4.

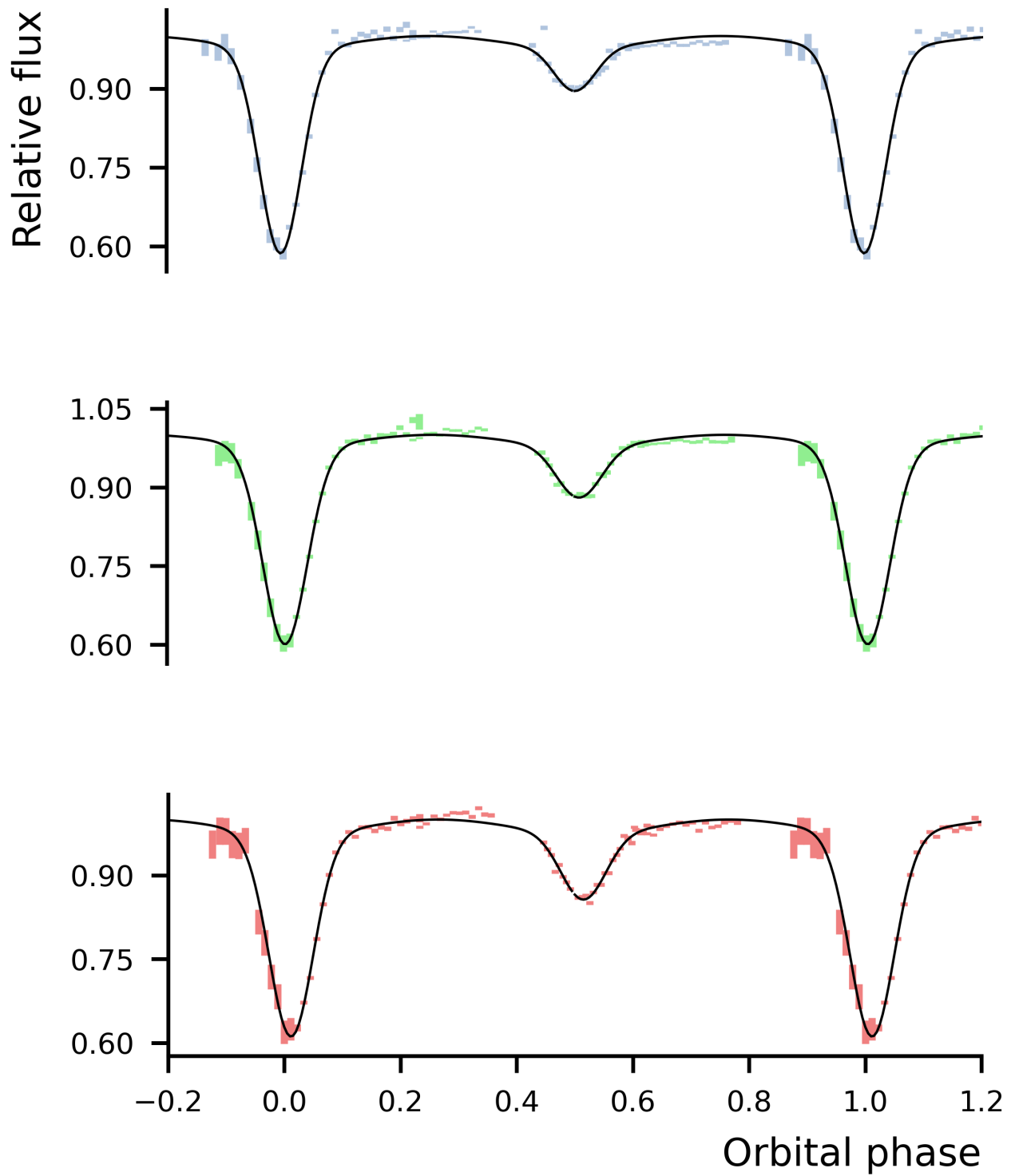


Figure 3.2: Lightcurve model of ASAS05.

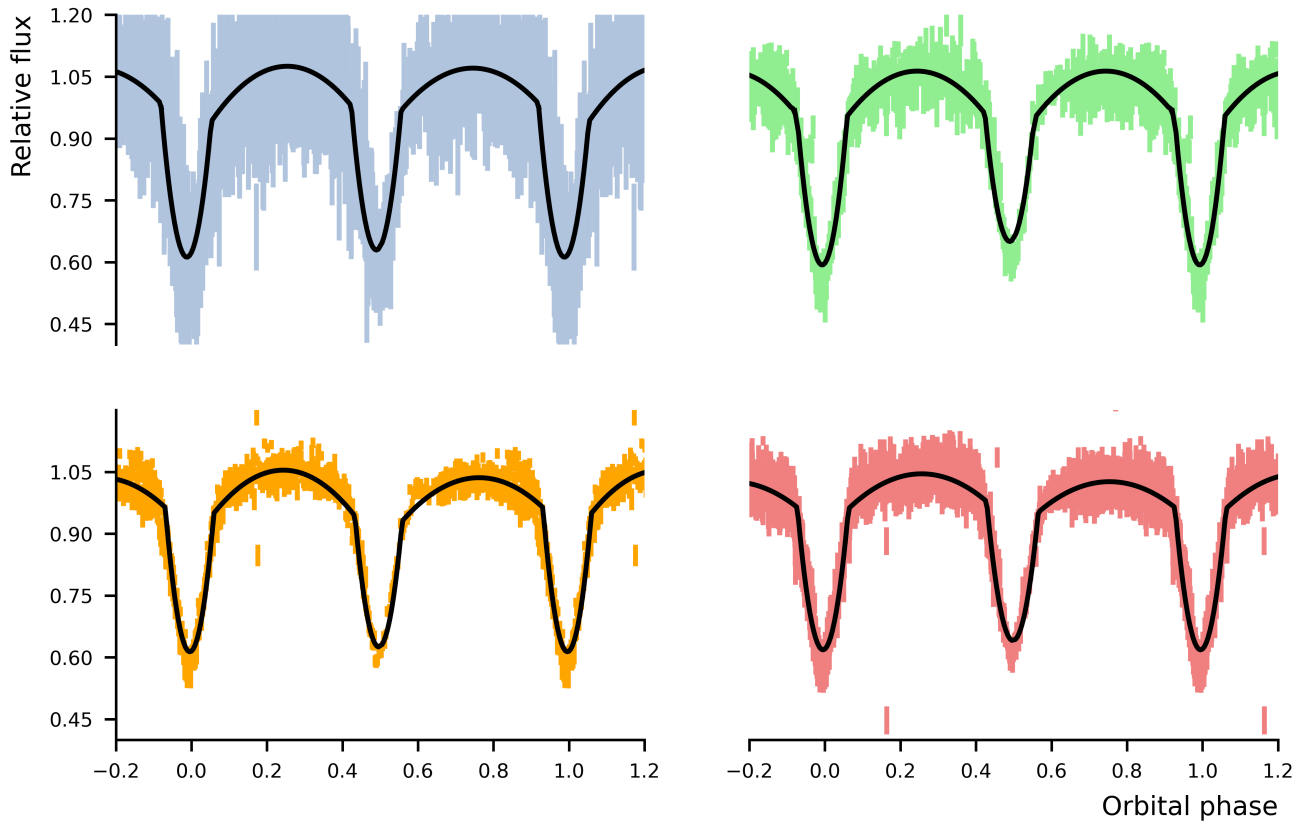


Figure 3.3: Lightcurve model of CRTS04.

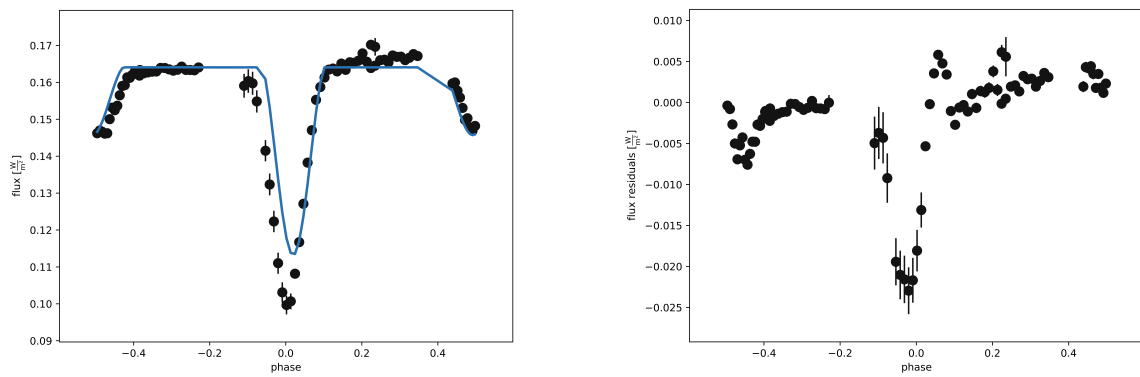


Figure 3.4: ASAS05 R band Nelder-Mead optimization and residuals.

Chapter 4

Results

En este capítulo se presentarán los resultados finales del trabajo y métodos usados para obtenerlos. Principalmente los parámetros orbitales y estelares determinados con el ajuste de las curvas de luz. Además se darán estimaciones y cotas para los valores que podrían venir dados por las curvas de velocidad radial.

No posterior distributions calculations were calculated for this reason so no the error later shown is not the true error but an estimation given by the standard deviation of the results.

4.1 Orbital and stellar parameters

The PHOEBE2 fitting returns values for most of the stellar parameters. However some of them are rough estimates given that without radial velocity curves no mass can be truly determined. The orbital parameters that are not present such as the semi major axis a and the longitude of the ascending node Ω could not be calculated given the lack of spectroscopic observations. The distance is directly taken from Gaia's database and is computed as the inverse of the parallax. As for the estimated stellar parameters, let us go over them one by one. The absolute magnitude, Mag , is calculated from.

$$\text{Mag} = \text{mag} - 2.5 \log_{10}(d) + 5 \quad (4.1)$$

Where d is the distance to the target. The first effective temperature is set to be that of Gaia. The second one is calculated by the fit from the effective temperature ratio. Assuming the star emits as a blackbody the Stefan-Boltzmann equation can be used which is given by.

$$L = 4\pi R^2 \sigma T^4 \quad (4.2)$$

Where $\sigma = 1.380649 \cdot 10^{-23} \text{m}^2 \text{kg} \text{s}^{-2} \text{K}^{-1}$ is Boltzmann's constant. For this work it is assumed that all stars are main sequence. This is because them being late type stars. This is also assumed for the A type component of ASAS05, however because this star is relatively massive it will evolve quicker and thus it may not necessarily be the case. Taking this assumption into account the mass of the primary star for both systems is assumed to fulfill the mass luminosity equation where $L \propto M^{\frac{3}{5}}$. If we take the values of

the primary star radius as known one can estimate the values of the secondary star radii with the radius ratio given by PHOEBE. Once all radii are known luminosity can be calculated with Equation 4.2 and afterwards using the mass-radius relation one can compute the values for the masses of all components.

The mass radius relation for main sequence stars with $M > 0.14 M_{\odot}$ is taken from Gorda and Svechnikov (1998) and is.

$$R = 1.25M^{0.65} \quad (4.3)$$

The mass radius relation for main sequence stars with $M < 0.14 M_{\odot}$ is.

$$R = 1.12M^{0.99} \quad (4.4)$$

The problem arises in the case of CRTS04 as the process of obtaining mass-radius relations in the case of M dwarfs is not fully established yet. The reason being that the relation used in the rest of the main sequence provides inconclusive results as linear fitting does not seem to be entirely accurate for very low mass stars. According to Cassisi and Salaris (2019) “recent empirical determinations of mass, effective temperature, and radius for a large sample of M dwarfs (M15, R19) have disclosed an apparent discontinuity in the T_{eff} -R diagram that corresponds to a mass $\sim 0.2 M_{\odot}$. R19 have hypothesised that the reason for this discontinuity is the transition to fully convective stars, although they did not perform any comparison with theory.” This was seen in the case of this work. The lightcurve fit, although accurate, provided a solution where the ratio of radii was seen as inconsistent, i.e. the radii were very different in the various filters and the ratio to the primary radius was too large of a difference to what could be expected from the lightcurve. For this reason we referred to Cassisi and Salaris (2019) T_{eff} -R relation. Those are the values present in Table 4.1.

In summary, for ASAS05 the radius of the primary is assumed to be known and taking into account the radius-ratio, the radius of the secondary is calculated. Using Equation 4.3 the mass is calculated for both. Finally the luminosity is computed using Equation 4.2. The values set for the primary radius are taken from Habets and Heintze (1981) and Pecaut and Mamajek (2013) where empirical relations are given.

In the case of CRTS04 a T_{eff} -R relation was used instead for both components due to lack of accuracy, the rest of the calculations are performed similarly to what was done for ASAS04. All final parameter fits and estimations are in Table 4.1.

	ASAS05			CRTS04			
	<i>V</i>	<i>R</i>	<i>I</i>	<i>g'</i>	<i>r'</i>	<i>i'</i>	<i>z'</i>
Orbital parameters							
T_0 [HJD]	2459892.5100 ± 0.0070	2459892.5100 ± 0.0070	2459892.5100 ± 0.0070	2459886.51600 ± 0.00032	2459886.51600 ± 0.00032	2459886.51600 ± 0.00032	2459886.51600 ± 0.00032
P [d]	0.7665 ± 0.0010	0.7665 ± 0.0010	0.7665 ± 0.0010	0.2170 ± 0.0040	0.2170 ± 0.0040	0.2170 ± 0.0040	0.2170 ± 0.0040
e	0.0410 ± 0.0040	0.0418 ± 0.0040	0.0333 ± 0.0040	0.0080 ± 0.0030	0.0080 ± 0.0030	0.0070 ± 0.0030	0.0020 ± 0.0030
i [deg]	75 ± 1	75 ± 1	77 ± 1	85.00 ± 0.50	84.50 ± 0.50	84.10 ± 0.50	85.20 ± 0.50
ω [deg]	178 ± 2	180 ± 2	174 ± 2	140 ± 15	130 ± 15	100 ± 15	110 ± 15
v [deg]	169 ± 2	173 ± 2	174 ± 2	350 ± 5	350 ± 5	350 ± 5	340 ± 5
D [pc]	1298 ± 30	1298 ± 30	1298 ± 30	364 ± 8	364 ± 8	364 ± 8	364 ± 8
Physical parameters							
Mag_1	3.493 ± 0.010	3.358 ± 0.010	3.528 ± 0.006	10.73 ± 0.040	10.73 ± 0.040	10.73 ± 0.040	10.73 ± 0.040
Mag_2	4.034 ± 0.010	3.851 ± 0.010	3.915 ± 0.010	13.513 ± 0.040	13.513 ± 0.040	13.513 ± 0.040	13.513 ± 0.040
T_{ratio}	0.500 ± 0.040	0.530 ± 0.040	0.600 ± 0.040	0.9300 ± 0.0090	0.9240 ± 0.0090	0.9371 ± 0.0090	0.9115 ± 0.0090
T_{eff1} [K]	7299 ± 20	7299 ± 20	7299 ± 20	3387 ± 12	3387 ± 12	3387 ± 12	3387 ± 12
T_{eff2} [K]	5140 ± 380	5140 ± 380	5324 ± 380	3180 ± 37	3130 ± 37	3170 ± 37	3090 ± 37
L_1^* [L_\odot]	7.73 ± 0.010	7.73 ± 0.010	7.73 ± 0.010	0.0130 ± 0.0020	0.0130 ± 0.0020	0.0130 ± 0.0020	0.0130 ± 0.0020
L_2^* [L_\odot]	0.54 ± 0.10	0.54 ± 0.10	0.54 ± 0.10	0.0050 ± 0.0010	0.0050 ± 0.0010	0.0050 ± 0.0010	0.0050 ± 0.0010
q^*	0.380 ± 0.050	0.360 ± 0.050	0.51 ± 0.10	0.80 ± 0.20	0.80 ± 0.20	0.80 ± 0.20	0.80 ± 0.20
M_1^* [M_\odot]	1.660 ± 0.010	1.660 ± 0.010	1.660 ± 0.010	0.290 ± 0.030	0.290 ± 0.030	0.290 ± 0.030	0.290 ± 0.030
M_2^* [M_\odot]	0.63 ± 0.10	0.610 ± 0.010	0.86 ± 0.12	0.220 ± 0.030	0.220 ± 0.030	0.220 ± 0.030	0.220 ± 0.030
R_{ratio}	1.87 ± 0.17	1.92 ± 0.17	1.53 ± 0.17	1.30 ± 0.30	1.30 ± 0.30	1.30 ± 0.30	1.30 ± 0.30
R_1^* [R_\odot]	1.738 ± 0.010	1.738 ± 0.010	1.738 ± 0.010	0.330 ± 0.030	0.330 ± 0.030	0.330 ± 0.030	0.330 ± 0.030
R_2^* [R_\odot]	0.920 ± 0.090	0.920 ± 0.090	1.10 ± 0.10	0.250 ± 0.030	0.250 ± 0.030	0.250 ± 0.030	0.250 ± 0.030

Table 4.1: All fitted and estimated (marked with an asterisk) parameters for both binary star systems.

The distance is obtained from Gaia parallax, Brown et al. (2021) and from this the absolute magnitudes. New ephemeris were also determined, rows 1 and 2 of Table 4.1. A new epoch is given and from the difference in predicted eclipse center timing and observed timing a new period is computed. For a comparison between the two see the old period at Table 2.1.

4.2 Classification and H-R diagram

From looking at the luminosities, temperatures and radii we can classify the stars according to Pecaut and Mamajek (2013). The types obtained for the primary and secondary of ASAS05 are respectively A9V and K2V. For CRTS04 these are M3V and M4.5V. One can plot these results in an HR diagram for a more intuitive visualization, see Figure 4.1. The rest of points are real stars obtained from the . All stars are main sequence stars, ASAS05 being an Algol type binary and CRTS04 a low mass ,apparently detached, short period M dwarf binary. The second one being much more interesting from a scientific standpoint.

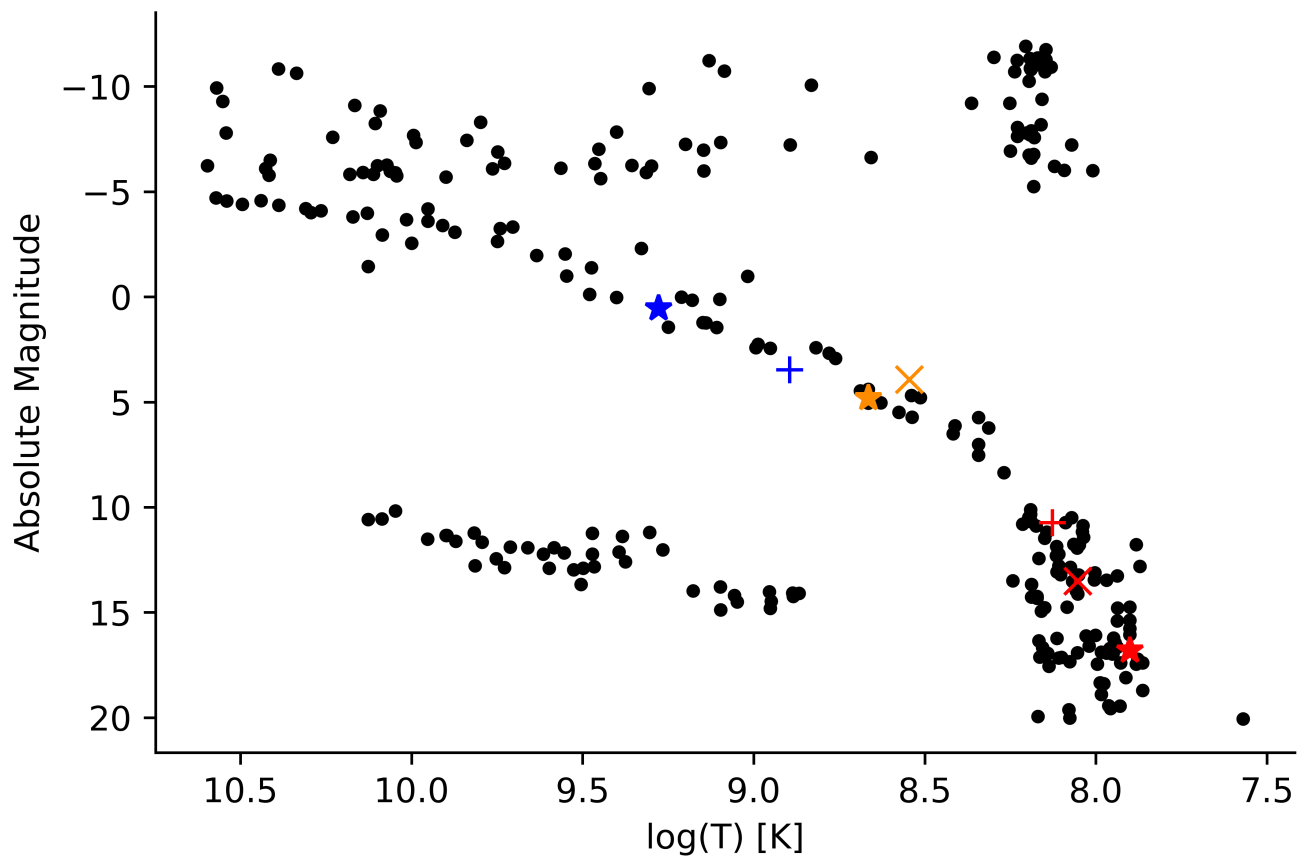


Figure 4.1: Visualization of a HR diagram, all star temperatures and magnitudes were obtained from the Gaia catalogue, Brown et al (2021). Absolute magnitudes were computed using the distance. Vega, the Sun and Alpha Centauri C were obtained from the literature. From left to right the colored stars are: Vega \star , ASAS05₁ $+$, the Sun \star , ASAS05₂ \times , CRTS04₁ $+$, CRTS04₂ \times and Alpha Centauri C \star ,

Chapter 5

Final conclusions

Finalmente en este capítulo se dan unas conclusiones, resumen de los resultados obtenidos y el trabajo que se quiere hacer en un futuro, esto incluye pedir tiempo de observación en telescopios con instrumentos de espectrografía para obtener curvas de velocidad radial.

5.1 Summary of the results obtained

Onsite and remote observations of a binary star have been planned and carried out during 4 nights with the IAC80 telescope of the Observatorio del Teide. The star ASASSN-VJ050229.84-052203.4 of adequate magnitude, period and coordinates was selected to observe during late 2022 and early 2023. Some light curves (V , R and I Johnson passbands) were obtained, these were well sampled in orbital phase.

In order to reduce and perform aperture photometry on ASASSN-VJ050229.84-052203.4 data two different reduction packages, PyRAF and PhotUtils, were used. In addition, different programs have been developed in Python to do data correction, astrometry, orbital phase calculation, light curve modelling and stellar and orbital parameters determination.

A very faint binary star, CRTSJ041918.8-071807, of approximately magnitude 17, that could not be observed with the IAC80 has also been remotely planned and observed with MuSCAT2. The reduction of this data has required the management of the MuSCAT2 pipeline using PyTransit, Parviainen (2015).

With the observed minimum times, new ephemeris have been determined for the two binaries. Although due to weather conditions it has not been possible to calibrate the observations of the two binaries. With data published in the literature, an estimate of the temperatures and spectral types of the two components of the system has been made which are in accordance to the results obtained by lightcurve modelling, both for ASASSN-VJ050229.84-052203.4 and in CRTSJ041918.8-071807.

These estimate results indicate that ASASSN-VJ050229.84-052203.4, as well as the shape of the light curves, is an Algol-like system with components A9V and K2V while CRTSJ041918.8-071807 is an interesting detached system with very low-mass components, M3V and M4.5V, $M < M_{\odot}$.

With initial values found in the literature, a preliminary adjustment has been made with Phoebe2. This has required installing the latest version of the program and learning how to use it in Python. The values found for the orbital parameters of the systems agree with what is expected from the observations.

In this work, Python as well as general and specific knowledge from the subjects of Computational Physics, Astrophysics and Cosmology, Astrophysical Techniques and Optics and Electronics in Astrophysics have been applied.

5.2 Future work

First of all, we would need to calibrate the two systems in a photometric night in order to obtain reliable colours. It would also be interesting to determine the spectral types of the two components with precision. It is important to take spectra to obtain radial velocity curves that allow us to reliably determine the value of the masses of the components.

Since CRTS04 is a relatively weak system it would be vital to obtain well-sampled light curves with a larger diameter telescope. CRTS04 is a very scientifically interesting system since to date it is one of the binaries with less massive components that has the one of the shortest known orbital periods. Obtaining curves in the IR would also be very useful, since in this spectral range the emission of these stars is predominant over the visible range. Although this binary is too weak to be able to observe time-resolved spectra with medium-sized telescopes, it would be very interesting to include it in an observation program with larger telescopes such as the Nordic Optical Telescope or the 3.5m Calar Alto observatory telescope.

New photometric data of the two binaries would allow us to refine the calculation of the ephemeris. With these data, new lightcurve models using Phoebe2 could be fit. Taking this into account and, also with a more in depth analysis and modelling of the current data using improved techniques, combined with the new data would allow for refinement of the parameters presented in this work.

References

- Christy, C. T. et al. (Jan. 2023). “The ASAS-SN catalogue of variable stars X: discovery of 116,000 new variable stars using G -band photometry”. In: *Monthly Notices of the Royal Astronomical Society* 519 (4), pp. 5271–5287. ISSN: 0035-8711. DOI: [10.1093/mnras/stac3801](https://doi.org/10.1093/mnras/stac3801).
- Hani, Mohammad et al. (Jan. 2014). “Physical And Orbital Parameter of the Visually Closed Binary System (HIP12552)”. PhD thesis.
- Taff, Lawrence G (May 1985). *Celestial mechanics*. en. Nashville, TN: John Wiley & Sons.
- Moulton, F R (June 1984). *An introduction to celestial mechanics*. Dover Books on Astronomy. Mineola, NY: Dover Publications.
- Martínez-Pais, Ignacio González (2003). *Introducción a la mecánica celeste: (formulación newtoniana)*. es.
- Murray, Carl D. and Alexandre C. M. Correia (Sept. 2010). “Keplerian Orbits and Dynamics of Exoplanets”. In.
- Sana, H., G. Rauw, and E. Gosset (Apr. 2001). “HD 152248: Evidence for a colliding wind interaction”. In: *Astronomy & Astrophysics* 370 (1), pp. 121–135. ISSN: 0004-6361. DOI: [10.1051/0004-6361:20010221](https://doi.org/10.1051/0004-6361:20010221).
- Eggleton, Peter (July 2006). *Evolutionary Processes in Binary and Multiple Stars*. Cambridge University Press. ISBN: 9780521855570. DOI: [10.1017/CB09780511536205](https://doi.org/10.1017/CB09780511536205).
- Huemmerich, S. and K. Bernhard (Oct. 2012). “New Eclipsing Binaries in the OGLE-II Database (Part 1). The Carina Galactic Disk Fields”. In: *Peremennye Zvezdy Prilozhenie* 12 (11).
- Jayasinghe, T et al. (July 2018). “The ASAS-SN catalogue of variable stars I: The Serendipitous Survey”. In: *Monthly Notices of the Royal Astronomical Society* 477 (3), pp. 3145–3163. ISSN: 0035-8711. DOI: [10.1093/mnras/sty838](https://doi.org/10.1093/mnras/sty838).
- Drake, A. J. et al. (Nov. 2011). “The Catalina Real-time Transient Survey”. In: DOI: [10.1017/S1743921312000889](https://doi.org/10.1017/S1743921312000889).
- Boch, T. and P. Fernique (Sept. 2013). “Astronomical Data Analysis Software and Systems XXIII”. In: ed. by N. Manset and P. Forshay. Astronomical Society of the Pacific Conference Series.
- Bonnarel, F. et al. (Apr. 2000). “The ALADIN interactive sky atlas”. In: *Astronomy and Astrophysics Supplement Series* 143 (1), pp. 33–40. ISSN: 0365-0138. DOI: [10.1051/aas:2000331](https://doi.org/10.1051/aas:2000331).
- Hog, E. et al. (Mar. 2000). “The Tycho-2 catalogue of the 2.5 million brightest stars”. In: *aap* 355, pp. L27–L30.
- Zacharias, N. et al. (Nov. 2005). “VizieR Online Data Catalog: NOMAD Catalog (Zacharias+2005)”. In: *VizieR Online Data Catalog*, I/297, pp. I/297.
- Johnson, Harold L. (Jan. 1966). “Astronomical Measurements in the Infrared”. In: *araa* 4, p. 193. DOI: [10.1146/annurev.aa.04.090166.001205](https://doi.org/10.1146/annurev.aa.04.090166.001205).
- Ochsenbein, F., P. Bauer, and J. Marcout (Apr. 2000). “The VizieR database of astronomical catalogues”. In: *Astronomy and Astrophysics Supplement Series* 143 (1), pp. 23–32. ISSN: 0365-0138. DOI: [10.1051/aas:2000169](https://doi.org/10.1051/aas:2000169).
- Papageorgiou, A. et al. (Aug. 2018). “An Updated Catalog of 4680 Northern Eclipsing Binaries with Algol-Type light curve morphology in the Catalina Sky Surveys”. In: DOI: [10.3847/1538-4365/aad8a9](https://doi.org/10.3847/1538-4365/aad8a9).
- Prieto, Marta (2004). “Caracterización nueva cámara CCD IAC80, mejora de telescopios nocturnos”. In.

- Narita, N. et al. (Dec. 2018). “MuSCAT2: four-color simultaneous camera for the 1.52-m Telescopio Carlos Sánchez”. In: *Journal of Astronomical Telescopes, Instruments, and Systems* 5 (01), p. 1. ISSN: 2329-4124. DOI: [10.1117/1.JATIS.5.1.015001](https://doi.org/10.1117/1.JATIS.5.1.015001).
- Parviainen, Hannu (Apr. 2015). “PyTransit: Fast and Easy Exoplanet Transit Modelling in Python”. In: DOI: [10.1093/mnras/stv894](https://doi.org/10.1093/mnras/stv894).
- Lang, Dustin et al. (May 2010). “ASTROMETRY.NET: BLIND ASTROMETRIC CALIBRATION OF ARBITRARY ASTRONOMICAL IMAGES”. In: *The Astronomical Journal* 139 (5), pp. 1782–1800. ISSN: 0004-6256. DOI: [10.1088/0004-6256/139/5/1782](https://doi.org/10.1088/0004-6256/139/5/1782).
- Skrutskie, M. F. et al. (Feb. 2006). “The Two Micron All Sky Survey (2MASS)”. In: *aj* 131.2, pp. 1163–1183. DOI: [10.1086/498708](https://doi.org/10.1086/498708).
- Landolt, Arlo U. (July 1992). “UBVRI Photometric Standard Stars in the Magnitude Range 11.5 < V < 16.0 Around the Celestial Equator”. In: *aj* 104, p. 340. DOI: [10.1086/116242](https://doi.org/10.1086/116242).
- Bajaj, V. and H. Khandrika (Apr. 2017). *Comparing Aperture Photometry Software Packages*. Space Telescope Science Institute.
- Prša, A. et al. (Dec. 2016). “PHYSICS OF ECLIPSING BINARIES. II. TOWARD THE INCREASED MODEL FIDELITY”. In: *The Astrophysical Journal Supplement Series* 227 (2), p. 29. ISSN: 1538-4365. DOI: [10.3847/1538-4365/227/2/29](https://doi.org/10.3847/1538-4365/227/2/29).
- Wilson, Robert E. and Edward J. Devinney (June 1971). “Realization of Accurate Close-Binary Light Curves: Application to MR Cygni”. In: *The Astrophysical Journal* 166, p. 605. ISSN: 0004-637X. DOI: [10.1086/150986](https://doi.org/10.1086/150986).
- Nelder, J. A. and R. Mead (Jan. 1965). “A Simplex Method for Function Minimization”. In: *The Computer Journal* 7 (4), pp. 308–313. ISSN: 0010-4620. DOI: [10.1093/comjnl/7.4.308](https://doi.org/10.1093/comjnl/7.4.308).
- Brown, A. G. A. et al. (May 2021). “Gaia Early Data Release 3”. In: *Astronomy & Astrophysics* 649, A1. ISSN: 0004-6361. DOI: [10.1051/0004-6361/202039657](https://doi.org/10.1051/0004-6361/202039657).
- Gorda, S. Yu and M. A. Svechnikov (Nov. 1998). “Determination of empirical mass-luminosity and mass-radius relations for main-sequence stars that are the components of eclipsing binary systems”. In: *Astronomy Reports* 42 (6), pp. 793–798.
- Habets, G. M. H. J. and J. R. W. Heintze (Nov. 1981). “Empirical bolometric corrections for the main-sequence.” In: *aaps* 46, pp. 193–237.
- Pecaut, Mark J. and Eric E. Mamajek (Sept. 2013). “Intrinsic Colors, Temperatures, and Bolometric Corrections of Pre-main-sequence Stars”. In: *apjs* 208.1, 9, p. 9. DOI: [10.1088/0067-0049/208/1/9](https://doi.org/10.1088/0067-0049/208/1/9). arXiv: [1307.2657](https://arxiv.org/abs/1307.2657) [astro-ph.SR].
- Cassisi, S. and M. Salaris (June 2019). “Effective temperature – radius relationship of M dwarfs”. In: *Astronomy & Astrophysics* 626, A32. ISSN: 0004-6361. DOI: [10.1051/0004-6361/201935468](https://doi.org/10.1051/0004-6361/201935468).